Demonstration of Type A volume Bragg gratings inscribed with a femtosecond Gaussian-Bessel laser beam

Joelle Harb, Lauris Talbot, Yannick Petit, Martin Bernier, Lionel Canioni

Research Article | Vol. 31, No. 10 / 8 May 2023 / Optics Express 15736
Optics EXPRESS

Demonstration of *Type A* volume Bragg gratings inscribed with a femtosecond Gaussian-Bessel laser beam

JOELLE HARB,[1] LAURIS TALBOT,[2] YANNICK PETIT,[1] MARTIN BERNIER,[2] AND LIONEL CANIONI[1,*]

[1] *University of Bordeaux, CNRS, ICMCB, UMR 5026, 87 avenue du Dr. A. Schweitzer, 33608 Pessac, Cedex, France*
[2] *Centre d'Optique, Photonique et Laser (COPL), Université Laval, Québec City, Québec G1V0A6, Canada*
[*] *Lionel.canioni@u-bordeaux.fr*

Abstract: To our knowledge, we report on the first demonstration of *Type A* VBGs inscribed in silver-containing phosphate glasses by femtosecond laser writing. The gratings are inscribed plane-by-plane by scanning the voxel of a 1030 nm Gaussian-Bessel inscription beam. This results in a refractive-index modification zone, induced by the appearance of silver clusters, extending over a much larger depth than those obtained with standard Gaussian beams. As a result, a high diffraction efficiency of 95% at 632.8 nm is demonstrated for a 2-µm period transmission grating with a 150-µm effective thickness indicating a strong refractive-index modulation of 1.78×10^{-3}. Meanwhile, a refractive-index modulation of 1.37×10^{-3} was observed at a wavelength of 1.55 µm. Thus, this work opens the avenue for highly effective femtosecond-written VBGs suitable for industrial applications.

1. Introduction

Volume Bragg gratings (VBGs) are optical devices having a 1-dimensional periodic refractive index modulation (Δn) that occupies a large volume inside of a transparent material. During recent decades, VBGs have been extensively used in free-space applications such as wavelength stabilization for laser diodes and both coherent and non-coherent high-power laser beam combinations [1]–[4]. So far, VBGs have been commonly fabricated in photo-thermo-refractive (PTR) glasses using CW (continuous wave) ultraviolet (UV) light illumination [5], [6]. Infrared femtosecond (fs) laser writing has also been employed more recently to address other materials such as oxide glasses (fused silica [7], [8], borosilicate [9]), chalcogenide and fluoride glasses [10], [11] and polymers (PMMA [12]). Indeed, fs laser pulses have gained interest due to their ability to induce local modifications inside non-photosensitive transparent materials by confining energy deposition thanks to nonlinear multi-photon absorption, as originally reported by Davis et *al.* in 1996 [13]. The creation of refractive-index change layers is usually achieved using tightly focused Gaussian laser beams and their depth is limited to the short confocal length of the focused beam. To obtain a VBG with an appropriate thickness with this approach, it is, therefore, necessary to stack multiple layers from bottom to top of the considered material [14]. This technique has significant drawbacks, such as long inscription times that linearly scale with the targeted depth of the VBG, as well as possible limitations regarding the homogeneity of the achieved periodicity when using this layer-by-layer approach alongside the line-by-line writing technique. As a result, the achieved experimental diffraction efficiencies are often lower than those expected as the required level of stability and positioning accuracy may not be maintained over the whole inscription volume. To overcome these limitations, VBGs have also been formed using Gaussian-Bessel laser beams. Indeed, a greater layer modification depth can be achieved, therefore reducing the required number of consecutive layers to inscribe and thus

#483722 https://doi.org/10.1364/OE.483722
Journal © 2023 Received 2 Jan 2023; revised 29 Mar 2023; accepted 12 Apr 2023; published 26 Apr 2023

Optics EXPRESS

leading to a faster recording time and a better efficiency [14]. Thus, the inscription of VBGs with fs Gaussian-Bessel laser beams has been reported in different materials: in fused silica, the multiplexing of 4 layers led to a 352 µm thick VBG with a ~90% diffraction efficiency at 633 nm, with a refractive index modulation Δn_{AC}, of 9.5×10^{-4} [15]; a 1 mm thick VBG in PTR glasses also achieved a diffraction efficiency of ~95% at 532 nm, with a refractive index modification around 2.3×10^{-4} [16]; and finally 2 mm thick VBGs in PMMA obtained after three days of inscription reached a diffraction efficiency of ~ 90% at 633 nm, with Δn_{AC} values from 0.5×10^{-4} to 5.0×10^{-4} [17].

In fact, there is a growing interest in inscribing VBGs in more photosensitive glass matrices enabling the generation of stronger refractive index modifications and accelerating the recording time of the inscription process. In particular, the phosphate glass family exhibits many attractive properties such as good chemical durability, ion exchangeability [18]–[20], especially with the addition of silver ions acting as a photosensitive support [21], [22]. In 2017, we showed the production of a novel type of positive refractive index modification based on the photochemistry of silver species [23], which has recently allowed to reach Δn values to 2×10^{-2} using the multi-scan approach [24]. This distinct modification is referred to as *Type A* for Argentum, related to the spatial distribution of the photo-induced silver clusters in the vicinity of the laser-glass interaction voxel [25], [26]. Indeed, this Δn is independent of the modifications of the glass matrix and shows two positive peaks for every laser writing line. In general, zinc phosphate glasses which allow for the laser-activated photochemistry of silver species, show near UV transparency and good oxidative properties to initially stabilize well dispersed silver ions. The overall transparency window of these photosensitized glasses covers the visible to the far end of the near-infrared (between 380 nm and 2700 nm), which allows for applications in this wavelength range. Thanks to the induced properties of the photo-inscribed silver clusters, several integrated photonics devices have been employed in such glasses, such as waveguides [23], couplers, beam splitters, refractive index sensors [27] and first-order waveguide Bragg gratings with periods down to 240 nm [28]. In such photosensitive glasses, Type-A modifications present more localized and smooth modifications allowing for a better preservation of the glass's optical quality [29].

In this paper, we report on what we believe is the first *Type A* VBG inscription in a commercial silver-containing glass (AG01, from Argolight). The VBGs were inscribed with femtosecond Gaussian-Bessel laser pulses with only a single layer. We demonstrate VBGs reaching high diffraction efficiency up to 95% at 632.8 nm with a period of 2 µm, and a 150 µm effective thickness indicating a 1.78×10^{-3} refractive index modulation according to simulations. The spectral selectivity is also investigated and shows good agreement with the numerical modeling. Moreover, the influence of the writing speed on the diffraction efficiency is analyzed. Finally, the VBG's diffraction efficiency is analyzed at 1.55 µm and shows a high refractive index modulation of 1.37×10^{-3}.

2. Experimental procedure

2.1. Inscription process

The Bessel beam is formed using the technique shown in Fig. 1(a). A UV-fused silica axicon (AX252-B, Thorlabs) having a physical angle of 2° enables the conversion of the incident Gaussian laser beam into a Gaussian-Bessel beam. The Bessel interference region (primary Bessel zone) after the axicon is expressed using the following formula:

$$Z_{max} = \frac{\omega_0 \cos(\alpha_0)}{\sin(\alpha_0)} \tag{1}$$

where Z_{max} represents the length of non-diffractive propagation. i.e., the depth of focus, α_0 is the cone half-angle and ω_0 is the incident beam radius.

Optics EXPRESS

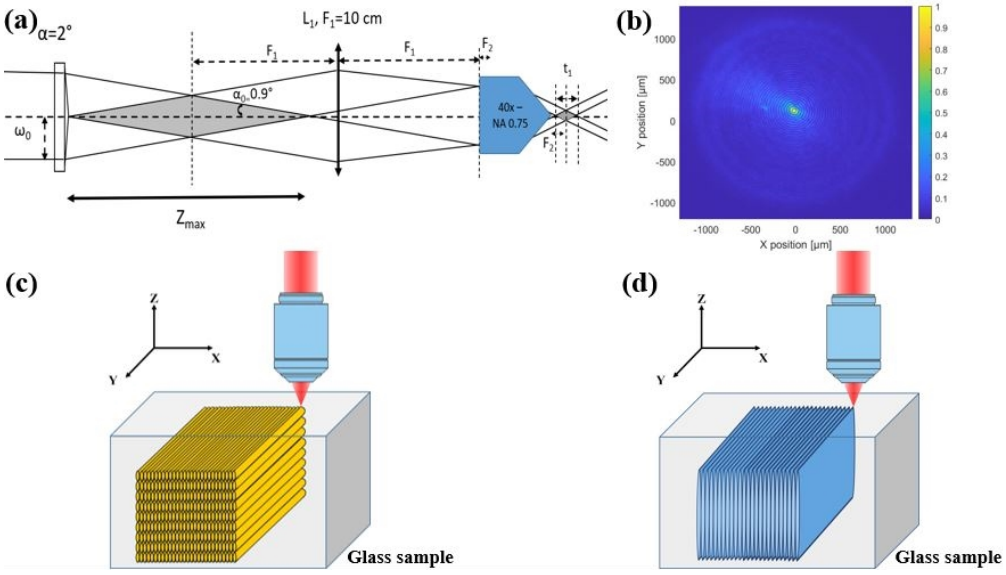

Fig. 1. (a) Schematic drawing of the experimental setup for the generation of the Gaussian-Bessel beam using an axicon and the demagnifying 4F optical system. (b) Experimental image profile of the intensity cross-section of the Gaussian-Bessel beam close to the $\frac{Z_{max}}{2}$ region. Schematic drawing of the volume Bragg gratings fabrication approaches: (c) Gaussian laser beam approach, (d) Gaussian-Bessel laser beam approach.

The central core radius of the primary Bessel beam ρ_0 (defined as the radial distance between the central intensity maximum and the first intensity minima) was calculated using the following equation:

$$\rho_0 = \frac{1.2024\lambda}{\pi \sin(\alpha_0)} \tag{2}$$

The incident Gaussian beam had a radius of 2.58 mm at 13.6% of maximal intensity. Using the formulas above, the dimensions of the primary Bessel beam were thus estimated to $Z_{max} = 166$ mm and $\rho_0 = 25.3$ µm.

Then, a 4F system is combined with the axicon to shorten the depth of field of the Bessel beam at the focal spot, and thus to increase the power density. This system involves the combination of a lens ($F_1 = 10$ cm) and an objective lens ($F_2 \sim 4.5$ mm, Nikon CFI Plan Fluor 40×- 0.75 NA) with the focal length ratio $\frac{F_1}{F_2} = 22.2$. The Bessel zone length is compressed by a factor of $(\frac{F_1}{F_2})^2$ after passing through the telescope, while the central core radius is reduced by $\frac{F_1}{F_2}$. The compressed Bessel beam (secondary Bessel region) showed a length of 336.3 µm with a central core radius of 1.14 µm. With such a long non-diffractive length, it is possible to inscribe volume Bragg gratings with sufficient thickness with only a single layer instead of having to superimpose many layers like when using a Gaussian beam, as shown in Fig. 1(c-d). Figure 1(b) presents the image profile of the intensity cross-section of the Gaussian-Bessel beam measured at a distance of ~10 cm after the axicon lens (near the $\frac{Z_{max}}{2}$ region). Note that the small beam to the left of the central beam is probably a parasitic Fresnel reflection. Theoretically, each ring of the Bessel beam (including the central lobe) contains the same amount of energy [30]. As the experimental measurement exhibits 40 rings, it shows that the energy in the central lobe of the beam is very weak compared to the total beam energy. An ideal Bessel beam of the nth order can be represented by:

$$E(r, \phi, z) = A_0 e^{(iK_z Z)} J_n(K_r r) e^{(\pm in\phi)} \tag{3}$$

Optics EXPRESS

where K_r and K_z are the radial and longitudinal wave vectors, respectively, and r is the radial coordinate.

For n = 0, the power contained in the Bessel beam up to radius b is calculated from [31]:

$$P = A_0^2 \int_0^{2\pi} \int_0^b J_0^2(rk_r) r dr d\phi = A_0^2 b^2 \pi \, (J_0(k_r b)^2 + J_1(k_r b)^2) \tag{4}$$

where b is the 40$^{\text{th}}$ zero of the zero function (in our case with 40 rings) and $k_r = \frac{2\pi \sin(\alpha_0)}{\lambda}$.

By measuring the power before the axicon and using Eq. (4) while considering the 40 rings existing in the Bessel beam, we calculate the peak intensity (or irradiance)A_0^2 in the center of the Bessel beam after the telescope, as shown below.

A ytterbium laser (Yuja, amplitude system) was used to realize the fs-DLW of VBGs. The circularly-polarized laser source operates at 1030 nm and delivers 417 fs pulses at a 1 MHz repetition rate, with a maximum average power of 10 W. The sample is a commercial silver-containing zinc-phosphate glass (AG01, Argolight) with a measured composition of 39.0P_2O_5-53.8ZnO-5.8Ag_2O-1Al_2O_3 (nominal cationic composition in mol%). While propagating from air to glass (n = 1.59), refraction extended the secondary Bessel beam to a length of 534 µm in the glass material [32]. The positioning of the sample during the laser inscription was assured within a precision of 30 nm by motorized 3-axis stages (XMS100 – VP5ZA, Newport). The grating transverse area was 400 × 400 µm^2 with a periodicity of 2 µm. VBGs were produced with their top position located at 160 µm below the surface for a series of writing velocities (20 µm/s – 60 µm/s – 80 µm/s). The periodicity of 2 µm was chosen for proof-of-concept of VBG inscription based on *Type A* modification, as it typically corresponds to the diameter of the inscribed structures with the chosen irradiation conditions in the regime of *Type A* inscription, as further detailed in Fig. 3 in Section 4. However, note that periodicities are not restricted to the diameter of the inscribed structures. In the chosen experimental conditions, the writing processes were typically achieved within 30 minutes to 1 hour, for velocities of 80 µm/s to 20 µm/s, respectively. In addition, VBGs were written with two average measured powers after the objective of 2.47 W and 2.59 W corresponding to estimated writing irradiances of 5.05 and 5.30 TW/cm^2, respectively, using Eq. (4), and leading to 2.47-2.59 µJ pulse energies. Note that these irradiances are similar to the values typically used for inscribing Type-A modifications with a standard Gaussian beam. Note that as Type A laser modifications are triggered at low laser irradiances, typically two orders of magnitude lower that the Type I regime threshold in such photosensitive glasses [29], the inscription beam propagation is not influenced by nonlinear effects. This is experimentally verified in Fig. 3(a) since, as shown by the silver clusters' fluorescence profile in depth, the energy deposition is smooth and in line with the expected propagation of a Gaussian-Bessel beam in linear regime.

2.2. Characterization of volume Bragg gratings

Diffraction efficiencies of all the inscribed VBGs were measured in transmission using a TEM_{00} He-Ne laser (632.8 nm wavelength) at the Bragg condition. The analyzed sample is positioned on a motorized rotation stage with an additional manual 3D translation stage. A lens of focal length F = 40 cm was chosen to loosely focus the beam inside the VBG, leading to an almost collimated propagation along the sample's thickness while having a beam diameter smaller than the VBG transverse area. For each angle detuning from the Bragg angle, we estimated the first-order Bragg diffraction efficiency as the ratio of the first-order diffracted beam power to the sum of the non-diffracted (zero order) power and the diffracted (first order) power. This relative diffraction efficiency is calculated as follows:

$$\eta_{Exp} = \frac{P_1}{P_1 + P_0} \tag{5}$$

In addition, diffraction efficiency was measured with a single-frequency fiber laser at 1.55 µm (FL-1550-SF, Changchun New Industries Optoelectronics Technology Co., Ltd.). The beam

Optics EXPRESS

from the fiber-coupled light source was collimated and traversed the same optical path described previously. Moreover, the spectral characteristics of the VBGs were analyzed using a broadband supercontinuum white light laser source (Sambda-450, Leukos). Then, the light was focused inside the glass bulk using the same setup as for the He-Ne laser. The transmitted light was refocused into an optical fiber (P400-1-SR) connected to a spectrometer (USB2000, Ocean Optics). We measured the transmission dip of the zeroth-order corresponding to both the first and second diffraction orders of the grating. The transmission spectra were normalized according to a spectrum obtained at normal incidence on the glass bulk inside the VBG's area.

3. Diffraction properties of volume Bragg gratings

Figure 2(a) shows the schematic representation of a transmitting Bragg grating inscribed in the volume of a photosensitive medium by sinusoidal modulation of the refractive index. The diffraction scheme represents the propagation of optical rays through the VBG, where the angle of the incident beam crosses the back surface and diffracts from θ_i to θ_d; while θ_i' and θ_d' are the incident and diffracted angles in medium, respectively. The VBG is characterized by the following set of parameters: the amplitude of refractive index modulation Δn_{AC}, the grating period Λ, the grating thickness d, the inclination or slant angle φ between the normal to the surface and the grating vector K_G, which is directed perpendicularly to the planes of a constant refractive index with a module of $K_G = \frac{2\pi\, m}{\Lambda}$; where m is the order of the VBG refractive-index modulation. The diffraction condition is analyzed using the momentum or K-space diagram method. Figure 2(b) illustrates the wave vectors k_i' and k_d' of the incident and diffracted waves, respectively. The vector relation is connected with a circle of radius $\beta = \frac{2\,\pi\, n}{\lambda}$ where n is the bulk index of refraction of the material and λ the wavelength in free space [33], [34]. The Bragg condition is satisfied for the corresponding vector equation as follows:

$$\overrightarrow{k_i}' + \overrightarrow{K_G} = \overrightarrow{k_d}' \tag{6}$$

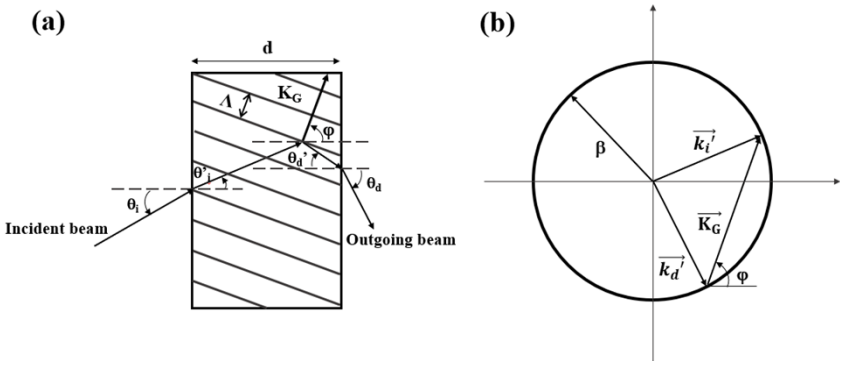

Fig. 2. (a) Diffraction representation of a transmission VBG. (b) Vector diagram for Bragg condition.

Therefore, diffraction of a beam with a certain wavelength occurs for only one angle, according to Bragg's condition:

$$|\cos(\varphi + \theta_i')| = \frac{K_G}{2\,\beta} = \frac{\lambda\, m}{2\, n\, \Lambda} \tag{7}$$

The diffraction efficiency of transmitting VBGs is modeled based on Kogelnik's coupled wave analysis [35] given by:

$$\eta = \frac{\sin^2\sqrt{\xi^2 + \upsilon^2}}{1 + \frac{\xi^2}{\upsilon^2}} \tag{8}$$

Optics EXPRESS

where ξ is the dephasing parameter describing the deviation from the Bragg condition and υ is the phase incursion that determines the maximum diffraction efficiency of VBG, written as:

$$\xi = \frac{d\left(K_G \cos\left(\varphi - \theta_i'\right) - \frac{K_G^2 \lambda}{4\pi n}\right)}{2\left(\cos\theta_i' - \frac{K_G}{\beta}\cos\varphi\right)} \tag{9}$$

$$\upsilon = \frac{\pi \Delta n_{AC}\, d}{\lambda\sqrt{\left(\cos\theta_i'\right)\left(\cos\theta_i' - \frac{K_G}{\beta}\cos\varphi\right)}} \tag{10}$$

4. Results and discussion

4.1. Glass modification

Lines of 200 µm in length were inscribed along the y-axis with the same laser parameters as those used to inscribe the VBGs described in Section 2.1. The side view fluorescence images (along the z-axis) have been acquired with a microscope (BX53, Olympus), using a camera (EP50, Olympus) and a 10× - 0.3 NA microscope objective (Olympus) with excitation light at 365 nm. Figure 3 shows the axial modification tracks produced by the Gaussian-Bessel beam, representing the traces of fluorescence composed of silver clusters. The longest depth of the modified tracks after inscribing one plane is around 300 µm when the writing speed is set to 20 µm/s. This value is slightly lower than the theoretical one of 534 µm (see Section 2.1), which is probably due to spherical aberrations or slight misalignment in the interference zone. Indeed, the creation of silver clusters and their associated fluorescence intensity depend strongly on the local laser inscription parameters. The fluorescence intensity is higher in the center of the modified track than on the tail and on the head. As recently demonstrated, Δn increases with increasing laser irradiance as it follows the growth of silver clusters [23]. Thus, the refractive index modification is also not fully homogenous along the z-axis. However, it is important to note that our glass maintains only *Type A* modification all along the axial depth. In contrast, the presence of both types I (smooth isotropic Δn) and II (anisotropic scattering centers) in fused silica using Gaussian-Bessel beams has been reported, which is related to the large variation of intensity along the modified structure and thus presenting a limitation to the diffraction efficiency of the VBG [36].

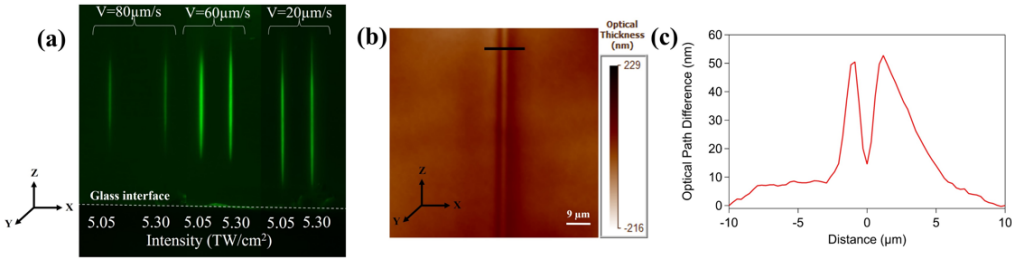

Fig. 3. (a) Side view microscopy fluorescence image (excitation at 365 nm) of modifications induced with the Gaussian-Bessel beam for different laser intensities and writing speeds. (b) Phase image of one laser-inscribed line (DLW parameters: 20 µm/sand 5.05TW/cm^2) taken from the lateral side of the sample, acquired through the SID4-Bio device. (c) Line profile of the typical OPD associated with the double-track *Type A* structures. Such line profile is extracted from a horizontal cross-section of the structure (black line in (b)).

The side-view image of one of these structures was collected using a 100× microscope objective (Zeiss) with 1.3 NA (used with a matching index oil n = 1.518) and the SID4-Bio sensor (Phasics)

Optics EXPRESS

plugged to an Axiovert 200 M Zeiss microscope. As represented in Fig. 3(b), this device allows for the construction of the phase image and the extraction of the local optical path difference (OPD) between the written lines and the pristine glass. Figure 3(c) shows an example of the OPD line profile with two high positive peaks of refractive index modification for an inscribed line at a velocity of 20 μm/s and irradiance of 5.05 TW/cm^2. Such double line changes are known as *Type A* modifications, associated to the photo-induced silver clusters at the periphery of the interaction voxel for every laser passage [23]. The inter-distance between the double lines was ~2 μm, which is approximately the size of the focalized laser beam diameter in our case. This distance can be adjusted by tuning the peak intensity, writing speed, or the numeral aperture of the objective. This also supported the choice of our VBGs' period (2 μm) as a double pass could have a period-homogenization effect. Moreover, due to the thickness of the inscribed line (200 μm), very large apparent lateral broadening of the *x*-axis line profile can be seen. This is usual for quantitative phase imaging measurement with thick phase object. Moreover, because these thick structures (thickness along the *y*-axis of Fig. 3(b)) may not be perfectly orthogonal to the glass interface, this may introduce an asymmetrical blurring effect, as seen in the right rail in Fig. 3(c). Abou Khalil et *al* [37]. recently published an approach allowing quantitative retrieval of the refractive index modification based on the measured OPD, especially for thick structures, by considering cylindrically-shaped volume modifications with varying diameters and heights. It has been shown that saturation behavior for the measured OPD occurs when structures become too thick. Such a depth-dependence and saturation depend also on the confocal length of the phase imaging conditions. Therefore, due to the shape difference (linear shapes with a diameter of 2 μm in our case), it is not possible to compare the OPD saturation level in our case with the work published in reference. Thus, the associated refractive index modification cannot be directly evaluated in our case, since the thickness is much larger than the effective length that can be coherently integrated with the phase imaging. However, we can roughly estimate from Fig. 3(c) a refractive index modification of the order of 5.8×10^{-3} for an estimated thickness of ~ 8 μm.

4.2. Characterization of VBGs

Figures 4 (a-b) show the experimental and simulated angular selectivity of the VBG inscribed with a period of 2 μm at 20μm/s with an irradiance of 5.05 TW/cm^2. As shown in Fig. 4(a), the experimental measurement demonstrates a peak transmission diffraction efficiency of ~95% at Bragg condition for an external incident Bragg angle of -21.7° at the wavelength of 632.8 nm. By fitting the experimental data with Eq. (8), the refractive index modulation Δn_{AC} and the effective thickness of the inscribed VBG were extracted. The measured data were best fitted with an effective thickness of 150 μm and index modulation $\Delta n_{AC} = 1.78 \times 10^{-3}$. In addition, this VBG was probed at the second diffraction order at an external Bragg angle of incidence of 6.17°. This grating exhibits a significant diffraction efficiency of ~65%, resulting in a modulated effective thickness of 165 μm and a slightly lower refractive index modulation $\Delta n_{AC} = 1.12 \times 10^{-3}$. This second-order diffraction is observed since the induced refractive index profile of the inscribed gratings is not a pure sinusoidal function, due to the highly nonlinear process of energy deposition during femtosecond laser inscription [38]. The VBG angular selectivity for the opposite orders was also measured. From the fitting of the experimental data, approximately similar values were obtained for the effective thickness as well as for the refractive index modification. Note that due to the moderate values of the incident and diffracted angles at the different diffraction orders, the correction of Fresnel reflections played no role in the measurements. Typically, a transmitting VBG with an inclination of $\varphi = \pm 90°$ is known as a symmetric grating or a normal grating. The direct modeling of our inscribed VBGs showed a needed slant angle of ~82.5° that allowed us to fully interpret the experimental incident angles.

In addition, the diffraction efficiency of all inscribed VBGs was measured for the first two Bragg orders to evaluate the influence of the different laser parameters. Their relative refractive

Optics EXPRESS

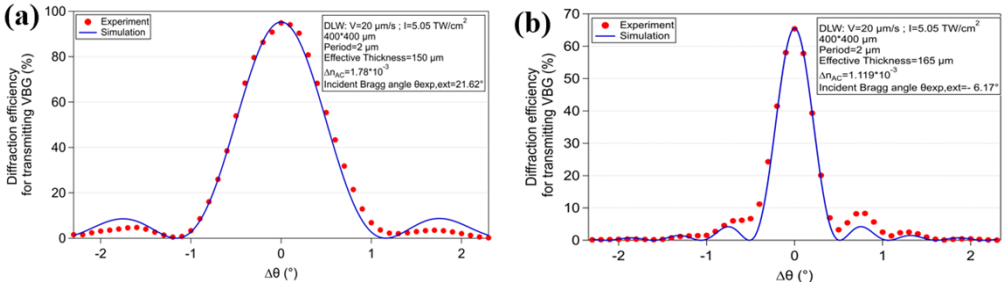

Fig. 4. Experimental and simulated dependence of the diffraction efficiency on the deviation from the Bragg angle of the transmitting Bragg grating for λ=632.8 nm: (a) incident Bragg angle = 21.62° (first order), (b) incident Bragg angle = -6.17° (second order).

index modification and effective thickness have been extracted from simulations. Note that VBGs inscribed with an irradiance of 5.3TW/cm^2 (as described in Section 2.1) were characterized showing approximately the same diffraction efficiencies as those inscribed with 5.05 TW/cm^2. The diffraction efficiency depended mostly on the writing velocity. Figure 5(a) summarizes the peak diffraction efficiency for the different writing speeds used to inscribe the VBGs. Their associated refractive index modification, extracted from the numerical simulation is represented in Fig. 5(b). The highest refractive index modification is obtained for the lowest writing speed (20 μm/s). This value decreases with the increase of speed during the inscription of VBGs. In addition, the second-order VBGs present lower refractive index modification for each VBG. The experimental measurements show that the effective thickness of the grating is approximately constant for all direct laser writing parameters (equal to 160 ± 7 μm for the first transmission order compared to 162 ± 9 μm for the second transmission order). Such effective thickness represents the effective longitudinal homogeneity of the in-depth refractive index modification, namely the longitudinal homogeneity that contributes efficiently to diffraction. We can notice that the axial length of the Gaussian-Bessel beam of the fluorescence images for excitation at 365 nm (Fig. 3(a)) depends on the laser inscription parameters. In fact, the thickness of the Δn_{AC} zone could be different than the axial length of the fluorescence for some laser inscription conditions. Indeed, silver clusters that mostly contribute to the refractive index modification may not be those being excited at 365 nm. Note that the lateral homogeneity of the line-by-line inscribed and associated periodicity is demonstrated *a posteriori* by the highly-efficient Bragg diffraction measurements and the great match between the experimental data and the model.

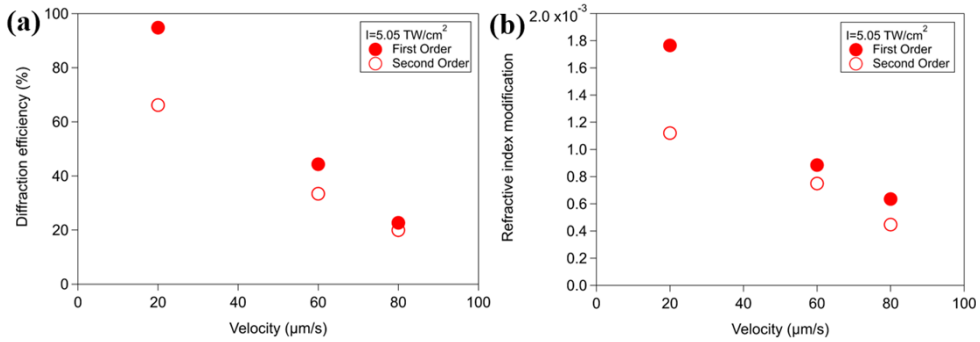

Fig. 5. (a) Peak diffraction efficiency measured for the first two Bragg orders of the inscribed VBGs at different writing speeds. (b) Their corresponding average refractive index modification extracted from the numerical simulations.

Optics EXPRESS

The spectral transmission dip of the zero-order corresponding to the first and the second diffraction order of the inscribed grating at 20 µm/s and 5.05 TW/cm^2 (as the VBG in Fig. 4) is presented in Figs. 6(a-b) for a VBG orientation at the Bragg angle for the 632.8 nm laser. The value of the first and second-order diffraction efficiency was obtained from the dip of the zero-order transmission spectrum, giving a diffraction efficiency of around 88.5% and 65.5%, respectively. The experimental result presents a good agreement with the simulation spectrum of the first and second diffraction order by assuming the same parameters as those used in Figs. 4(a-b).

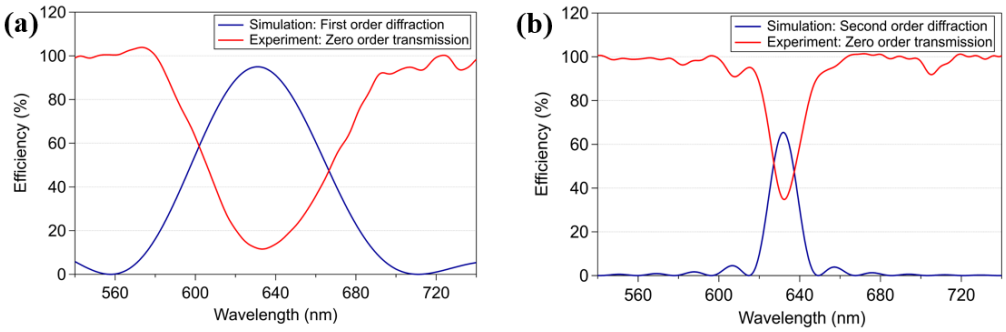

Fig. 6. Measured transmission dip of the zero-order in the case of (a) the first and (b) the second Bragg order. Simulation of the diffraction spectra for the corresponding orders of the VBG.

Finally, the diffraction efficiency has also been investigated for a Bragg angle adjusted to the wavelength of a 1.55 µm laser. The first-order transmission spectrum of the inscribed grating at 20 μm/s and 5.05 TW/cm^2 (as the VBG in Fig. 4(a)) showed a diffraction efficiency of ~17%. By fitting the angular spectrum, we were able to infer an effective thickness of 150 µm and a peak Δn_{AC} value of 1.37×10^{-3}. Accordingly, both the maximal diffraction efficiency and the photo-induced refractive index modulation decreased at a 1.55 µm wavelength. Theoretically, simulating the Bragg diffraction efficiency at 1.55 µm using the parameters extracted in Fig. 4(a) would have yielded a diffraction efficiency of 28.5%. Thus, one can conclude that most of the observed decrease in diffraction efficiency is inherently due to the increase in the tested wavelength while the refractive index modification shows only a weak dispersion decrease from 1.78×10^{-3} at 633 nm down to 1.37×10^{-3} at 1.55 µm. Thus, the high refractive index modulation persists in the near-infrared range. However, longer gratings around 360 ~ 460 µm will be investigated in the future to obtain higher diffraction efficiencies in the infrared range.

5. Conclusion

In conclusion, *Type A* VBGs have been demonstrated for the first time and reached a diffraction efficiency of ~95% in transmission at 632.8 nm. Single plane gratings with a period of 2 µm were inscribed in commercial silver-containing phosphate glasses with a Gaussian-Bessel femtosecond beam. This approach led to long modification lengths, allowing to speed up the inscription process and optimize the period homogeneity over the grating depth. In addition, experimental measurements showed the presence of second-order diffraction with significant efficiency. The spectral characteristics also exhibited good agreement with the numerical simulation. Moreover, our gratings were successfully investigated at 1.55 µm, showing that the refractive index modification remains high enough to achieve efficient diffraction in the near-infrared region. Thus, in the future, inscribing these *Type A*–based periodic structures in the recently synthesized silver-doped gallo-germanate glasses exhibiting enhanced transmission into the mid-infrared (MIR) range offers new insights and advantages for the fabrication of VBGs

Optics EXPRESS

into the MIR range [39]. The most efficient grating was recorded in ~1 hour at a writing speed of 20 $\mu m/s$. Also, switching to a higher repetition rate with faster velocities is very promising for high throughput. Furthermore, using the multi-scan approach would increase the refractive index modification of the inscribed VBGs. In addition, recent lasers with higher repetition rates (up to the GHz regime) in burst mode would still allow for reaching the *Type-A*-modification irradiance threshold while shortening the VBGs' writing time by delivering the needed multi-pulse energy deposition to inscribe efficient VBGs.

Funding. Conseil Régional Aquitaine (AAPR2020-2019-8193110); Agence Nationale de la Recherche (19-CE08-0021-01); Société d'Accélération du Transfert de Technologies (Volume Bragg Gratings project); Horizon 2020 Framework Programme ((Marie Skłodowska-Curie grant agreement No 823941); Natural Sciences and Engineering Research Council of Canada (CRDPJ-543631-19).

Acknowledgments. Authors would like to thank Bruno Bousquet for lending the spectrometer and the premium-grade optical fiber and Patrick Mounaix for lending the single frequency fiber laser at 1.55 µm.

Disclosures. The authors declare no conflicts of interest.

Data availability. Data underlying the results presented in this paper are not publicly available at this time but may be obtained from the authors upon reasonable request.

References

1. A. Sevian, O. Andrusyak, I. Ciapurin, V. Smirnov, G. Venus, and L. Glebov, "Efficient power scaling of laser radiation by spectral-beam combining: erratum," Opt. Lett. **33**(7), 760 (2008).
2. D. Richter, M. P. Siems, W. J. Middents, M. Heck, T. A. Goebel, C. Matzdorf, R. G. Krämer, A. Tünnermann, and S. Nolte, "Minimizing residual spectral drift in laser diode bars using femtosecond-written volume Bragg gratings in fused silica," Opt. Lett. **42**(3), 623 (2017).
3. I. V. Ciapurin, L. B. Glebov, L. N. Glebova, V. I. Smirnov, and E. V. Rotari, "Incoherent combining of 100-W Yb-fiber laser beams by PTR Bragg grating," in *Advances in Fiber Lasers*, SPIE, 209–219, (2003).
4. O. G. Andrusyak, "Dense spectral beam combining with volume bragg gratings in photo-thermo-refractive glass," These de doctorat, Bordeaux 1, 2009. Accessed: 2022. [Online]. Available: https://www.theses.fr/2009BOR13779
5. L. A. Siiman, J. Lumeau, L. Canioni, and L. B. Glebov, "Ultrashort laser pulse diffraction by transmitting volume Bragg gratings in photo-thermo-refractive glass," Opt. Lett. **34**(17), 2572 (2009).
6. O. M. Efimov, L. B. Glebov, L. N. Glebova, K. C. Richardson, and V. I. Smirnov, "High-efficiency Bragg gratings in photothermorefractive glass," Appl. Opt. **38**(4), 619 (1999).
7. K. Yamada, W. Watanabe, K. Kintaka, J. Nishii, and K. Itoh, "Volume Grating Induced by a Self-Trapped Long Filament of Femtosecond Laser Pulses in Silica Glass," Jpn. J. Appl. Phys. **42**(Part 1, No. 11), 6916–6919 (2003).
8. C. Voigtländer, D. Richter, J. Thomas, A. Tünnermann, and S. Nolte, "Inscription of high contrast volume Bragg gratings in fused silica with femtosecond laser pulses," Appl. Phys. A **102**(1), 35–38 (2011).
9. D. Grobnic, S. J. Mihailov, C. W. Smelser, M. Becker, and M. W. Rothhardt, "Femtosecond laser fabrication of Bragg gratings in borosilicate ion-exchange waveguides," IEEE Photon. Technol. Lett. **18**(13), 1403–1405 (2006).
10. D. G. MacLachlan, R. R. Thomson, C. R. Cunningham, and D. Lee, "Mid-Infrared Volume Phase Gratings Manufactured using Ultrafast Laser Inscription," Opt. Mater. Express **3**(10), 1616–1624 (2013).
11. L. Talbot, D. Richter, M. Heck, S. Nolte, and M. Bernier, "Femtosecond-written volume Bragg gratings in fluoride glasses," Opt. Lett. **45**(13), 3625–3628 (2020).
12. Y. Matushiro, S. Juodkazis, K. Hatanaka, and W. Watanabe, "Regenerated volume gratings in PMMA after femtosecond laser writing," Opt. Lett., OL **42**(8), 1632–1635 (2017).
13. K. M. Davis, K. Miura, N. Sugimoto, and K. Hirao, "Writing waveguides in glass with a femtosecond laser," Opt. Lett. **21**(21), 1729–1731 (1996).
14. A. S. Chernikov, R. V. Chkalov, and D. G. Vasilchenkova, "Volume Bragg Grating Fabrication by Femtosecond Laser Pulses," in *2020 International Conference Laser Optics (ICLO)*, 1 (2020).
15. M. Mikutis, T. Kudrius, G. Šlekys, D. Paipulas, and S. Juodkazis, "High 90% efficiency Bragg gratings formed in fused silica by femtosecond Gauss-Bessel laser beams," Opt. Mater. Express **3**(11), 1862–1871 (2013).
16. Y. J. Zhang, G. D. Zhang, C. L. Chen, R. Stoian, and G. H. Cheng, "Transmission volume phase holographic gratings in photo-thermo-refractive glass written with femtosecond laser Bessel beams," Opt. Mater. Express **6**(11), 3491–3499 (2016).
17. W. Watanabe, "Regeneration of a Grating in PMMA Inscribed by Femtosecond Laser Bessel Beam," J. Laser Micro/Nanoeng. **12**(2), 102–106 (2017).
18. J. H. Campbell and T. I. Suratwala, "Nd-doped phosphate glasses for high-energy/high-peak-power lasers," J. Non-Cryst. Solids **263-264**(264), 318–341 (2000).
19. N. G. Boetti, D. Pugliese, E. Ceci-Ginistrelli, J. Lousteau, D. Janner, and D. Milanese, "Highly Doped Phosphate Glass Fibers for Compact Lasers and Amplifiers: A Review," Appl. Sci. **7**(12), 1295 (2017).
20. K. Bourhis, "Photostructuration par laser infrarouge femtoseconde de verres photosensible de phosphate de zinc, d'argent et de gallium," Bordeaux University, France, 2011.

Optics EXPRESS

21. Y. Petit, S. Danto, T. Guérineau, A. Abou Khalil, A. Le Camus, E. Fargin, G. Duchateau, J.-P. Bérubé, R. Vallée, Y. Messaddeq, T. Cardinal, and L. Canioni, "On the femtosecond laser-induced photochemistry in silver-containing oxide glasses: mechanisms, related optical and physico-chemical properties, and technological applications," Adv. Opt. Technol. **7**(5), 291–309 (2018).
22. S. D. Stookey, "Photosensitive Glass," Ind. Eng. Chem. **41**(4), 856–861 (1949).
23. A. Abou Khalil, J.-P. Bérubé, S. Danto, J.-C. Desmoulin, T. Cardinal, Y. Petit, R. Vallée, and L. Canioni, "Direct laser writing of a new type of waveguides in silver containing glasses," Sci. Rep. **7**(1), 11124–9 (2017).
24. L. Loi, Y. Petit, Y. Petit, and L. Canioni, "High refractive index change in Type A laser modification using a multi-scan approach," Opt. Mater. Express **12**(6), 2297–2308 (2022).
25. M. Bellec, A. Royon, B. Bousquet, K. Bourhis, M. Treguer, T. Cardinal, M. Richardson, and L. Canioni, "Beat the diffraction limit in 3D direct laser writing in photosensitive glass," Opt. Express, OE **17**(12), 10304–10318 (2009).
26. M. Bellec, A. Royon, K. Bourhis, J. Choi, B. Bousquet, M. Tréguer, T. Cardinal, J.-J. Videau, M. Richardson, and L. Canioni, "3D Patterning at the Nanoscale of Fluorescent Emitters in Glass," J. Phys. Chem. C **114**(37), 15584–15588 (2010).
27. A. Abou Khalil, P. Lalanne, J.-P. Bérubé, Y. Petit, R. Vallée, and L. Canioni, "Femtosecond laser writing of near-surface waveguides for refractive-index sensing," Opt. Express **27**(22), 31130 (2019).
28. R. Laberdesque, L. Loi, T. Guérineau, A. Abou Khalil, S. Danto, T. Cardinal, L. Canioni, and Y. Petit, "Three-dimensional femtosecond laser inscription of Type A-based high-efficiency first-order waveguide Bragg gratings," J. of Advanced Optical Technologies, vol. to appear in press, (2023).
29. A. Abou Khalil, J.-P. Bérubé, S. Danto, T. Cardinal, Y. Petit, L. Canioni, and R. Vallée, "Comparative study between the standard type I and the type A femtosecond laser induced refractive index change in silver containing glasses," Opt. Mater. Express **9**(6), 2640–2651 (2019).
30. "Bessel Beam Generation," *Photon Engineering*. https://photonengr.com/fred-software/application-examples/bessel-beam/ (accessed Oct. 06, 2022).
31. P. Birch, I. Ituen, R. Young, and C. Chatwin, "Long Distance Bessel Beam Propagation Through Kolmogorov Turbulence," J. Opt. Soc. Am. A **32**(11), 2066 (2015).
32. K. Liao, W. Wang, X. Mei, J. Cui, M. Li, and X. Li, "An analytical model to predict the sizes of modified layer in glass with femtosecond Bessel beam," Optik **185**, 232–241 (2019).
33. I. V. Ciapurin, "Modeling of phase volume diffractive gratings, part 1: transmitting sinusoidal uniform gratings," Opt. Eng **45**(1), 015802 (2006).
34. L. Siiman, "Ultrashort Laser Pulse Interaction With Photo-thermo-refractive Glass," University of Central Florida, Orlando, Florida, 2008. [Online]. Available: https://stars.library.ucf.edu/etd/3725.
35. H. Kogelnik, "Coupled wave theory for thick hologram gratings," The Bell Syst. Tech. J. **48**(9), 2909–2947 (1969).
36. D. Paipulas, M. Mikutis, V. Sirutkaitis, and S. Juodkazis, "Volumetric modifications in fused silica using Gaussian and Bessel femtosecond laser beams," *presented at the SPIE/SIOM Pacific Rim Laser Damage: Optical Materials for High-Power Lasers,*, Shanghai China, J. Shao, T. Jitsuno, and W. Rudolph, Eds., Shanghai, China, 87860D, (2013).
37. A. Abou Khalil, W. Gebremichael, Y. Petit, and L. Canioni, "Refractive index change measurement by quantitative microscopy phase imaging for femtosecond laser written structures," Opt. Commun. **485**, 126731 (2021).
38. C. W. Smelser, S. J. Mihailov, and D. Grobnic, "Characterization of Fourier components in type I infrared ultrafast laser induced fiber Bragg gratings," Opt. Lett. **32**(11), 1453–1455 (2007).
39. T. Guérineau, A. Fargues, J. Lapointe, R. Vallée, Y. Messaddeq, L. Canioni, Y. Petit, and T. Cardinal, "Laser Direct Writing of Silver Clusters-Based Subwavelength Periodic Structures Embedded in Mid-Infrared Gallo-Germanate Glass," Adv. Photonics Res. **3**(10), 2200032 (2022).